Electronic supplementary information:

Numerical simulation and high-speed photographic study on the audio-frequency noise in the analytical ICP source

Yundong Xie[1], Yongyang Su[2*], Zhiming Li[2], Lihua Zhai[2], Xiaofei Lan[1*], Wei Wang[2], Jiang Xu[2]

1. School of Physics and Astronomy, China West Normal University, Nanchong, Sichuan, 637002, China. E-mail: lan-x-f@163.com
2. Northwest Institute of Nuclear Technology, P.O. box 69-14, Xi'an, Shaanxi, 710024, China. E-mail: suyongyang@nint.ac.cn

1 Theory and model

1.1 Temperature and velocity

As in previous numerical simulations[31,32,35,37,38,41], we assume the analytical ICP source is in the local thermodynamic equilibrium (LTE) state. Consider ICP as a conductive fluid that satisfies the conservation equations for energy and momentum[38]

$$\rho C_p \frac{\partial T}{\partial t} + \rho C_p \cdot \nabla T + \nabla \cdot q = Q \quad ()$$

$$\rho (u \cdot \nabla) u = \nabla \cdot [-pI + K] + F \quad ()$$

where ρ is the fluid density, C_p is the heat capacity at constant pressure, T is temperature, t is time, q is the heat flow vector, u is the fluid velocity, p is the total pressure, I is the unit tensor, K is the stress tensor in addition to the pressure. The heat source (Q) and the Lorentz force (F) are defined as

$$Q = E \cdot J + \frac{\partial}{\partial T}\left(\frac{5}{2} \cdot \frac{k_B T}{q}\right)(\nabla T \cdot J) + Q_{rad} \quad ()$$

$$F = J \times B \quad ()$$

The heat source consists of Joule heat, enthalpy change and volume radiation loss. The enthalpy change is equal to the heat of the reaction at constant pressure. As the ionization degree of Ar in the ICP source is found to be very low[31,42,45], the effect of enthalpy change on heat transfer could be ignored. The current is defined as

$$J = \sigma(E + u \times B) \quad ()$$

where σ is the electrical conductivity. The electromagnetic field inside the torch can be determined by solving Maxwell's equations. The spatial distributions of temperature and gas velocity inside the ICP torch in steady-state can be obtained by calculating the above equations.

1.2 Particle number density

The ionization degree of Ar in the analytical ICP is <0.04%[31,42,45], so only the primary ionization of Ar atom is considered here. The plasma components can be calculated by solving the Saha equation[46]

$$\frac{n_e\, n_i}{n_0} = 2 \cdot \frac{\zeta_i}{\zeta_0} \cdot \left(\frac{2\pi m_e k_B T}{h^2}\right)^{3/2} \cdot exp\left(-\frac{E_i - \Delta E_i}{k_B T}\right) \quad ()$$

where n_0, n_i, and n_e are the number densities of the atom, ion, and electron, respectively. ζ_0 and ζ_i are the partition functions of the corresponding atom and ion, respectively. m_e is the electron mass, k_B is the Boltzmann constant, h is the Planck constant, and E_i is the ionization energy of the lower ionization state. ΔE_i is a reduction in ionization energy due to the non-ideal effect and could be neglected under the conditions investigated here. For pure Ar-ICP in the LTE state, n_e=n_i. According to the ideal gas equation of state, n_e+n_0=p/($k_B T$). The number density distributions of each particle could be determined by solving the above equations.

2 Simulation method

Since the 2010s, numerical studies on the analytical ICP source in the absence (called "Case 1") and presence (called "Case 2") of an interface have been conducted and verified preliminarily by Bogaerts et al.[1–6] using ANSYS FLUENT®. Earlier, spatial distributions of electron temperature, electron number density and gas kinetic temperature in ICP with an interface (named "Case 3") were diagnosed experimentally

by Hieftje et al. using Thomson scattering and Rayleigh scattering technique[7–11]. In the above studies, standard Fassel-type torches were used. For comparison and verification, we simulated the fundamental parameters of the Ar-ICP source, same as those cases and then compared them with the literature values.

The ICP torch with an interface is assumed to be 2D axisymmetric, as shown in Fig. E1. The dimensions and operating conditions are compiled in Table E1 and Table E2, respectively. The simulations in this paper were performed by COMSOL® v5.6. To accelerate convergence, the total radial and axial length of the simulation area are greater than the torch's outer radius. The sample gas, auxiliary gas, and coolant gas are pure argon flows. The r.f. power with a frequency of 27.12 MHz is coupled to the load coil to heat the gas flows until a sudden change in conductivity occurs, igniting a gas discharge. The inlets for sample gas, auxiliary gas and coolant gas were set as velocity inlets with fully developed laminar flow.

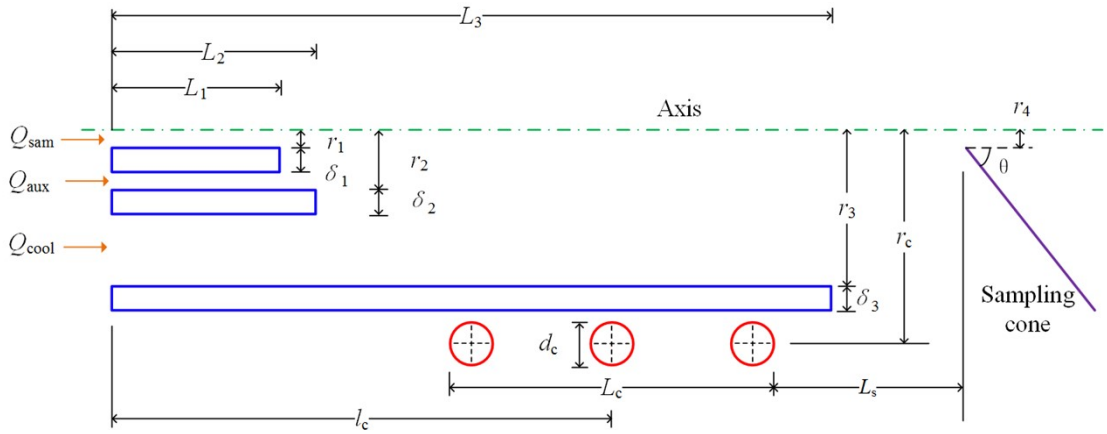

Fig. E1 2D axisymmetric schematic (not in scale) of the ICP torch in the presence of a sampling cone. r_i, δ_i, L_i – the inner radius, wall thickness and length of a tube, i=1, 2, 3 for central tube, intermediate tube and outer tube, respectively. r_4 – the radius of the sampling orifice, θ - the inclination angle of the windward side, L_s – the sampling depth in the unit of mm above load coil (ALC); d_c – the diameter of the coil tube, l_c – the distance of the coil centre from the torch inlet, r_c, L_c – the winding radius and total length of the coil, respectively. Q_{sam} – sample gas flow rate, Q_{aux} – auxiliary gas flow rate, Q_{cool} – coolant gas flow rate.

Table E1 Dimensions of the Fassel-type torch and the sampling cone

No.	Case 1[12]	Case 2[6]	Case 3[†8,9]	Torch "a"	Torch "b"	Section "Dependence of the pulsation frequency on the sampling depth"	Section "Suppression mechanism of using a bonnet"
r_1/mm	0.5	0.75	0.5	0.75	0.75	0.75	0.5
δ_1/mm	2	1.75	2	1.75	1.75	1.75	1
L_1/mm	7.2	7.2	7.2	7.2	7.2	7.2	7.2
r_2/mm	7	7	7	6	7	7	7
δ_2/mm	1	1	1	1	1	1	1
L_2/mm	10	10	10	10	10	10	10
r_3/mm	9	9	9	8	9	9	9
δ_3/mm	1	1	1	2	1	1	1
L_3/mm	35	35	35	35	35	35	35
d_c/mm	3	3	3	3	3	3	3
L_c/mm	19	19	19	18	18	17	18
l_c/mm	22	22	22	19.5	19.5	22.5	22
r_c/*mm*	12.5	12.5	13	12	12	12	12.5
With interface?	No	Yes	No	No	No	Yes	Yes
With bonnet?	No	No	Yes	No	Yes	no	Yes
r_4/mm	-	0.5	-	-	-	0.45	0.5
θ	-	70°	-	-	-	45°	70°

Table E2 Operating conditions of the ICP source

	Case 1[12]	Case 2[6]	Case 3[8,9]	Section "Experimental"	Section "Dependence of the pulsation frequency on the sampling depth"	Section "Suppression mechanism of using a bonnet"
r.f. frequency /MHz	27.12					
r.f. power /kW	1.0	1.0	1.25	1.2	1.4	1.4
Q_{cool} /L min^{-1}	16	12	15	13	15	16
Q_{aux} /L min^{-1}	1	0.4	1	1	1	1
Q_{sam} /L min^{-1}	0-0.8	1	0.6-1.4	1	1	1
L_s /mm ALC	-	10	13	-	10-35	10

3 Simulation results

3.1 Case 1

As a starting study in their group, Lindner et al.[12] simulated the effective temperature inside the central channel and the mean flow velocity inside the plasma without an interface. For verification, the temperature inside the central channel was diagnosed experimentally from the end-on collected line-to-background ratio with varying Q_{sam}. Meanwhile, the flow velocity inside the coil region was determined by

side-on observation of analyte emission with individual monodisperse droplet introduction. The geometric parameters and operating conditions were compiled as "Case 1" in Table E1 and Table E2, respectively.

We simulated this case using the proposed method. The radial and axial lengths of the calculation area are 50x50 mm. The peak value of temperature on the axis, as well as the flow velocity in two flow paths (labelled as "path 1" and "path 2"), were retrieved under varying Q_{sam} conditions. In Fig. E2a, both the simulations and experimental results indicate that the maximum temperature on the axis decreases with increasing Q_{sam} in the range of 0-0.8 L/min. The simulated temperature in this work agrees with the experimental value within the reported uncertainty (±3%RSD). Fig. E2b shows that our simulated velocity for "path 2" is ~14.29% greater than the experimental value. In contrast, our simulation for "path 1" lies between the observed value and the simulation reported by Lindner et al.

(a)

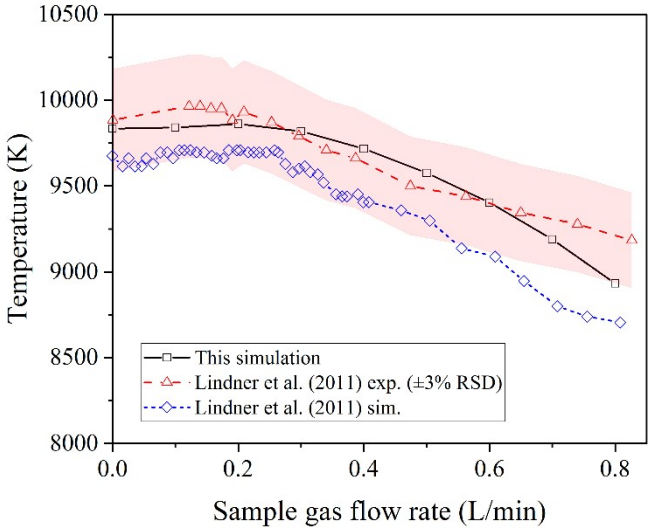

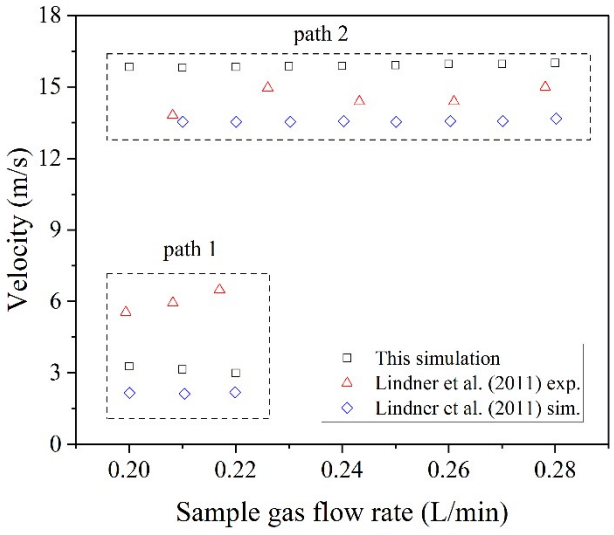

Fig. E2 Comparison of temperature (a) and velocity (b) simulated in this work with the literature values[12].

3.2 Case 2

Subsequently, Bogaerts et al. continued to refine the relevant model and reported a series of simulation studies[2–5]. In their tutorial review[6], 2D profiles of temperature, electron number density and gas flow velocity were calculated for ICP with the presence of a sampling cone. Compared with Case 1, the inner diameter and wall thickness of the central tube in Case 2 were changed from 0.75 to 0.5 mm and from 1.75 mm and 2 mm, respectively, while other geometric parameters were the same, as illustrated in Table E1. The corresponding operating conditions are presented in Table E2.

Case 2 was simulated with a calculation area of 50x45 mm in radial and axial length. Some assumptions were made: (1) the temperature at the sampling cone was set at 500 K[6]; (2) the pressure at the sampling orifice was set at -14 kPa (atmospheric pressure of 101 kPa as reference pressure)[13]; (3) Solid heat transfer exists in the outer tube of which the outer boundary is thermal insulation. After ignition of around 60 s, the temperature of the outer tube becomes stable (~700 K), which is in agreement with an infrared observation[14]. The influence of the temperature of the outer tube on the plasma parameters was found to be insignificant. The spatial distributions of temperature, electron number density and gas velocity obtained from this simulation were similar to those reported by Bogaerts and Aghaei[6], as shown in Fig. E3.

In Fig. E3a from Bogaerts and Aghaei[6], a hot region within 9000-10000 K is continuous upstream of the sampling cone (4 mm ALC to 10 mm ALC), and no cool central channel is observed. The simulation result is inconsistent with the experimentally observed radial profiles of electron temperature and gas-kinetic temperature in ICP with an interface[7–9]. The spatial distribution of temperature obtained by our simulation seems more reasonable, as shown in Fig. E3b.

Comparing Fig. E3c and E3d, a central channel exist in both simulations. However, the maximum value of electron number density (n_e) reported by Bogaerts and Aghaei[6] is three times our simulation (5×10^{21} m^{-3}). Our simulation value of n_e is comparable with the experimental values determined under typical operating conditions by different groups using various techniques[7–9,15–17].

Temperature (K):

(a) (b)

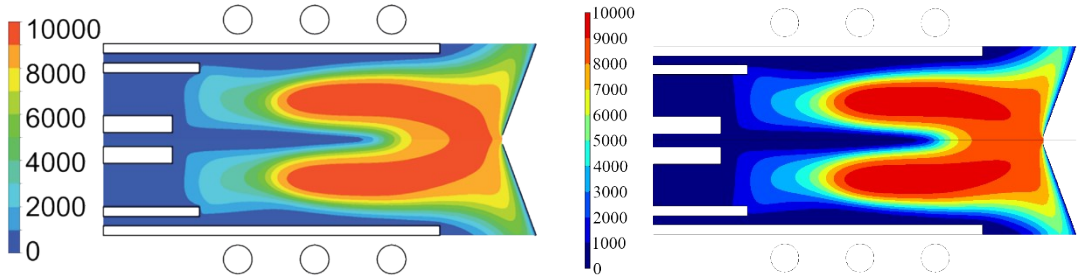

Electron number density (m^{-3}):

(c) (d)

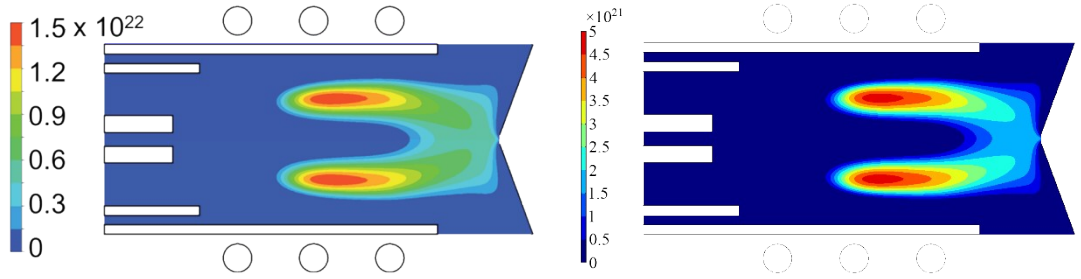

Velocity (m/s):

(e) (f)

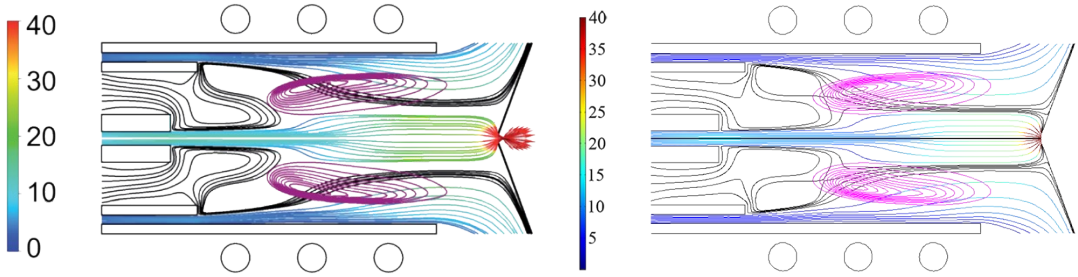

Fig. E3 Comparison of spatial distributions of temperature, electron number density and gas velocity simulated from Bogaerts and Aghaei[6] (a, c, e) and this work (b, d, f).

3.3 Case 3

Using Thomson and Rayleigh scattering techniques, Gamez et al. (2007)[8,9] measured the fundamental parameters (electron temperature, electron number density, gas kinetic temperature) of ICP under varying operating conditions. Unfortunately, no dimensions of the torch were given in their papers.[8,9]. For simplicity, we used the dimensions of a torch in the absence of an interface (see Case 3 in Table E1) for simulation. The operating conditions are illustrated in Table E2. The radial profiles of electron number density (n_e) and electron temperature (T_e) at an observation height of 7 mm ALC were simulated in this work and then compared with the experimental values reported by Gamez et al. (2007)[9].

Fig. E4 shows symmetry both in radial profiles of n_e and T_e from simulation and experiment. Experimental curves of electron temperature and gas-kinetic temperature (T_g) in the induction zone are in agreement, demonstrating that plasma in this area is in the LTE state, as shown in Fig. E4a. To elucidate the discrepancies between the simulation and experimental values, we summarized the variations of n_e and T_e with operating conditions in the induction zone and the central channel by reviewing previous literature, as illustrated in Table E3.

In the induction region, n_e and T_e at a radial position of 4 mm and observation height of ~7 mm ALC increases with r.f. power because energy from the r.f. source mainly deposits here. The dependencies of n_e and T_e on sample gas flow rate (Q_{sam}) and water load seem very weak. The reason is that the gas flow passing through this region is mainly from the auxiliary gas and the coolant gas but not from the sample gas, as

shown in Fig. E3e and E3f. The situation in the central channel is more complicated when a solution is introduced. The experimental curves reported by Gamez et al.[8,9] were obtained when 19 mg/min water was loaded, but the effect of water load on n_e and T_e was not evaluated. To verify the proposed method, we only compare the parameters from the simulation with the experimental value in the introduction zone. Radial profiles of n_e and T_e under varying Q_{sam} and r.f. power were simulated and plotted in Fig. E4.

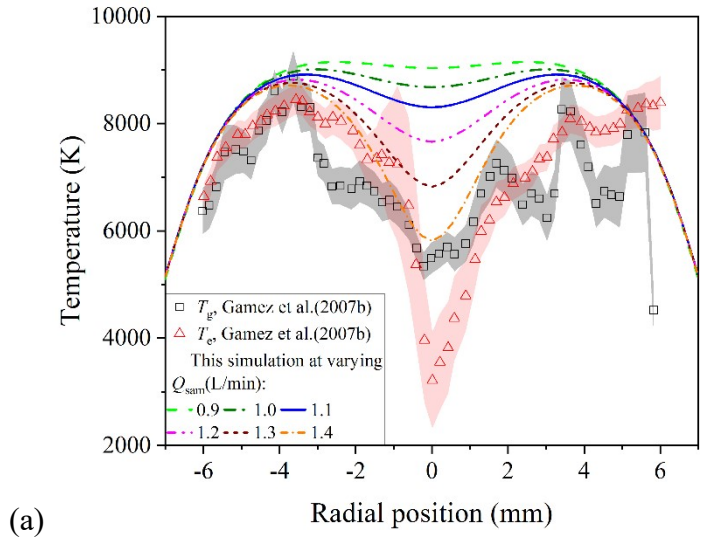

(a)

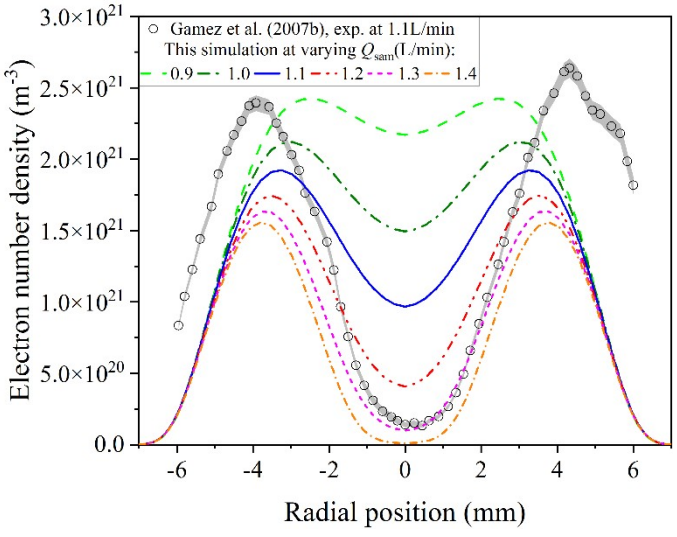

(b)

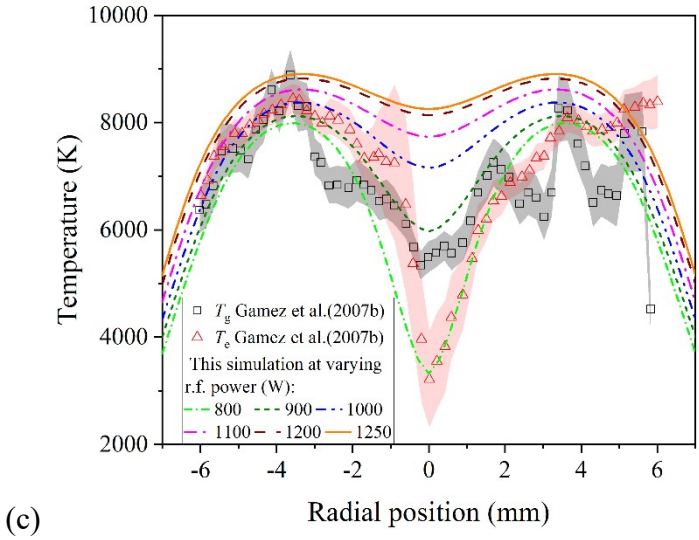

(c)

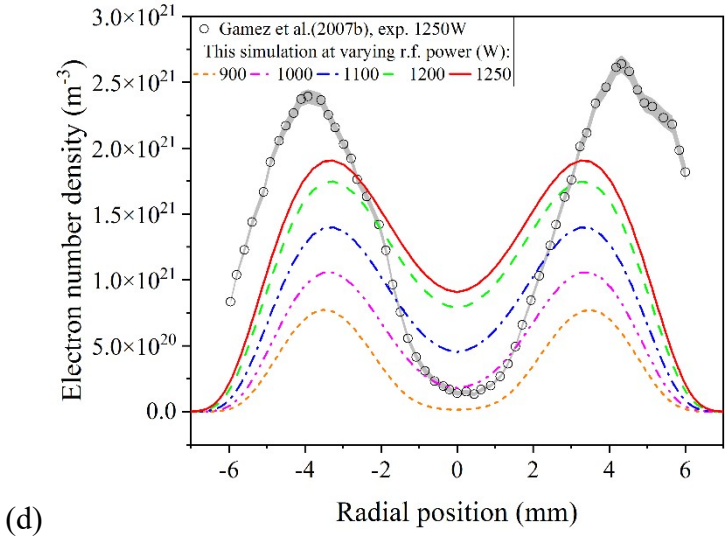

(d)

Fig. E4 Radial profiles of electron number density and electron temperature simulated under varying Q_{sam} (a, b) and r.f. power (c, d) when no interface is present. Observation height: 7 mm ALC, sampling depth: 13 mm ALC. The uncertainty of the experimental value was displayed using the measurement precision obtained under similar condition[8].

Table E3 Summary of the variations of n_e and T_e with operating conditions in the induction zone and the central channel

Radial position	Parameter	r.f. power	Q_{sam}	Water load	Observation height (mm ALC)
Induction zone	n_e	+[8,10]	/[9]	/[10]	8-20: -[10],

					10-20: -[11], 6-8: -[7], 13-17: -[9]
(r=4 mm)	T_e	+[8,10]	-[9]	/[10]	10-20: -[11], 6-8: /[7], 13-17: /[9]
Central channel (r=0 mm)	n_e	+[8,10]	-[9]	-[10]	5-25: /[10], 10-20: /[11], 6-8: /[7], 13-17: /[9]
	T_e	+[8,10]	-[9]	-[10]	10-20: -[11], 6-8: -[7], 13-17: -[9]

+: increase with the parameter; -: decrease with the parameter; /: independent of the parameter.

Fig. E4a shows that T_e at a radial position of 4 mm (centre of the introduction zone) drops slightly when Q_{sam} increases from 0.9 L/min to 1.4 L/min. The simulated value of T_e (8833 K) is 600 K higher than the experimental value under the same Q_{sam} (1.1 L/min); hence the relative difference is calculated to be 7.3%. When Q_{sam} increases, the peak position of n_e moves away from the axis while the peak value drops significantly, as indicated in Fig. E4b. The peak value of n_e and n_e at a radial position of 4 mm are 20% and 26% lower than the experimental peak value (2.40×10^{21} m^{-3}). Fig. E4c and E4d show that T_e and n_e increase with r.f. power. The trend is consistent with the experimental findings illustrated in Table E3.

4 Reference

1 H. Lindner and A. Bogaerts, *Spectrochim. Acta Part B At. Spectrosc.*, 2011, **66**, 421–431.

2 M. Aghaei, H. Lindner and A. Bogaerts, *J. Anal. At. Spectrom.*, 2012, **27**, 604–610.

3 M. Aghaei, H. Lindner and A. Bogaerts, *Spectrochim. Acta - Part B At. Spectrosc.*, 2012, **76**, 56–64.

4 M. Aghaei, H. Lindner and A. Bogaerts, *J. Anal. At. Spectrom.*, 2013, **28**, 1485–1492.

5 M. Aghaei, L. Flamigni, H. Lindner, D. Günther and A. Bogaerts, *J. Anal. At. Spectrom.*, 2014, **29**, 249–261.

6 A. Bogaerts and M. Aghaei, *J. Anal. At. Spectrom.*, 2017, **32**, 233–261.

7 S. A. Lehn, K. A. Warner, M. Huang and G. M. Hieftje, *Spectrochim. Acta - Part B At. Spectrosc.*, 2002, **57**, 1739–1751.

8 G. Gamez, S. A. Lehn, M. Huang and G. M. Hieftje, *Spectrochim. Acta - Part B At. Spectrosc.*, 2007, **62**, 357–369.

9 G. Gamez, S. A. Lehn, M. Huang and G. M. Hieftje, *Spectrochim. Acta - Part B At. Spectrosc.*, 2007, **62**, 370–377.

10 M. Huang, D. S. Hanselman, P. Yang and G. M. Hieftje, *Spectrochim. Acta Part B At. Spectrosc.*, 1992, **47**, 765–785.

11 P. Yang, J. A. Horner, N. N. Sesi and G. M. Hieftje, *Spectrochim. acta, Part B At. Spectrosc.*, 2000, **55**, 1833–1845.

12 H. Lindner, A. Murtazin, S. Groh, K. Niemax and A. Bogaerts, *Anal. Chem.*, 2011, **83**, 9260–9266.

13 R. L. Spencer, J. Krogel, J. Palmer, A. Payne, A. Sampson, W. Somers and C. N. Woods, *Spectrochim. Acta - Part B At. Spectrosc.*, 2009, **64**, 215–221.

14 C. Engelhard, A. Scheffer, T. Maue, G. M. Hieftje and W. Buscher, *Spectrochim. Acta - Part B At. Spectrosc.*, 2007, **62**, 1161–1168.

15 R. S. Houk and Y. Zhai, *Spectrochim. Acta - Part B At. Spectrosc.*, 2001, **56**, 1055–1067.

16 S. M. Javid, S. Alavi, X. Guo, A. Zabihihesari and J. Mostaghimi, *Spectrochim. Acta - Part B At. Spectrosc.*, 2021, **180**, 106182.

17 A. Montaser, *Inductively coupled plasma mass spectrometry*, John Wiley, 1998.